Electrochimica Acta 283 (2018) 1037–1044

Contents lists available at ScienceDirect

Electrochimica Acta

journal homepage: www.elsevier.com/locate/electacta

Electrochemical reduction of carbon dioxide on copper-based nanocatalysts using the rotating ring-disc electrode

Xuanheng Zhu [a], Kalyani Gupta [b], Marco Bersani [b], Jawwad A. Darr [b], Paul R. Shearing [a], Dan J.L. Brett [a, *]

[a] Electrochemical Innovation Lab, Department of Chemical Engineering, Torrington Place, University College London, London, WC1E 7JE, UK
[b] Department of Chemistry, Christopher Ingold Building, 20 Gordon Street, University College London, London, WC1H 0AJ, UK

ARTICLE INFO

Article history:
Received 24 March 2018
Received in revised form
27 June 2018
Accepted 6 July 2018
Available online 7 July 2018

Keywords:
Electrochemical reduction of carbon dioxide
Rotating ring-disc electrode
Continuous hydrothermal flow synthesis
Copper(I) oxide
Nanoparticles

ABSTRACT

A continuous hydrothermal flow synthesis method was used to produce copper(I) oxide nanoparticles, which were used as an electrocatalyst for the reduction of CO_2. A rotating ring-disc electrode (RRDE) system was used to study the electroreduction processes, including a systematic study (including quantitative NMR analysis) to identify product species formed at the disc and detected at the ring. In 0.5 M $KHCO_3$ electrolyte with a pH of 7.1, carbon dioxide was found to be exclusively reduced to formate. In the potential range −0.5 to −0.9 V vs the reversible hydrogen electrode (RHE), an active material/glassy-carbon disc electrode was shown to produce formate, with a maximum Faradaic efficiency of 66% (at −0.8 V vs RHE).

1. Introduction

The amount of carbon dioxide (CO_2) in the atmosphere has increased dramatically due to the combustion of fossil fuels, with potentially catastrophic effects caused by global warming [1,2]. Various methods have been proposed to capture or use CO_2 from the atmosphere, including the use of CO_2 absorbing plants and algae (photo-synthesis), thermochemical reactions, and photo-catalytic and electrochemical reactions [3]. Some of these methods allow the chemical conversion of CO_2 into small molecules, which themselves can be used as fuel. For example, methanol and formic acid can be produced from the reduction of CO_2 using graphene-loaded TiO_2 catalyst under photocatalytic conditions [4].

The products obtained from the electro-reduction of CO_2 depend on the catalyst, electrolyte, electrode potential and pH/media used [5]. The range of product species from CO_2 reduction include methane, methanol, formic acid, formaldehyde, and carbon monoxide, which themselves can be used as fuels for subsequent power generation [6].

A range of catalysts have previously been studied for the electroreduction of CO_2, these include platinum, silver, gold, copper, copper oxides, etc. [7]. Le et al. investigated an electrodeposited cuprous oxide catalyst for the reduction of CO_2 to methanol in 0.5 M $KHCO_3$ electrolyte [8]. Methanol was produced with the highest Faradaic efficiency of 38% being obtained at −1.5 V vs SCE (Standard Calomel Electrode). The same authors also used other copper or copper oxide electrocatalysts, including air-oxidised Cu, anodised Cu, and electrodeposited cuprous oxide films, where electro-deposited cuprous oxide films gave the best results. Other researchers have additionally used a co-catalyst for the reduction of CO_2; for example, Ohya et al. coated copper oxide onto Zn metal to generate methane and ethylene with 300 mmol dm^{-3} KOH in methanol as both catholyte and anolyte [9]. Without copper oxide particles, only formic acid and carbon monoxide were detected; however, with copper(I) oxide, methane and ethylene were generated from electrochemical reduction of CO_2 with efficiencies of 7.5 and 6.8%, respectively. In addition, copper(I) oxide was found to be more active than copper(II) oxide when combined with Zn. Ren et al. found that ethylene and ethanol were obtained as the major products from CO_2 electrochemical reduction using Cu_2O films deposited on Cu discs when in 0.1 M $KHCO_3$ electrolyte. The Faradaic efficiency was observed to be in the range 34–39% for ethylene and 9–16% for ethanol, respectively [10].

* Corresponding author.
E-mail address: d.brett@ucl.ac.uk (D.J.L. Brett).
URL: http://www.ucl.ac.uk/eil

https://doi.org/10.1016/j.electacta.2018.07.025

Compared to bulk copper oxide films or powders, nanoparticles have much higher surface area to volume ratios and consequently, may possess greater activity. The nanoparticle synthesis method has an effect on the efficacy of any CO_2 electroreduction approach and the conversion efficiency obtained. Continuous Hydrothermal Flow Synthesis (CHFS) is a rapid and flexible method for producing inorganic nanoparticles at high pressure and temperature, and was reviewed recently by some of the authors [11]. The size of the nanoparticles can be affected by changing the concentration of the precursors, the flow rate of the solutions, the pressure and the temperature applied to the system [12]. Additionally, capping agents can also be added to the process to make charge stabilised or sterically stabilised nanoparticles. A wide range of metal oxide nanoparticles can be produced via the CHFS method [11,13]. Bersani et al. has synthesized highly monodispersed CuO nanoparticles with diameter of 11 nm using a CHFS method. CuO catalyst has been used for CO_2 hydrogenation [14]. Copper oxide nanomaterials made via the CHFS process also hold great promise as tuneable catalysts for CO_2 electroreduction that can be fabricated at large scale. CHFS was used to make ultra-fine copper(II) oxide nanoparticles that were used for the electrocatalytic reduction of CO_2 to formic acid at high Faradaic efficiencies. Gupta et al. has used CuO nanoparticles as electrocatalyst in a Nafion ink for the electroreduction of CO_2. The highest Faradaic efficiency for formic acid production (61%) was observed with a 25 wt% Nafion fraction, at a potential of −1.4 V *vs* Ag/AgCl [15].

Copper oxide modified electrodes have been investigated as a function of applied electrode potential using *in situ* infra-red spectroscopy and *ex situ* Raman and X-ray photoelectron spectroscopy [16]. In deoxygenated $KHCO_3$ electrolyte, bicarbonate and carbonate species were found to adsorb to the electrode during reduction and the CuO was reduced to Cu(I) or Cu(0) species. Carbonate was incorporated into the structure and CuO starting material was not regenerated on cycling to positive potentials. In contrast, in CO_2 saturated $KHCO_3$ solution, surface adsorption of bicarbonate and carbonate was not observed and adsorption of a carbonate-species was observed with *in situ* infrared spectroscopy. On cycling to negative potentials, larger reduction currents were observed in the presence of CO_2; however, less of the charge could be attributed to the reduction of CuO. In the presence of CO_2, CuO underwent reduction to Cu_2O and potentially Cu, with no incorporation of carbonate. Under these conditions the CuO starting material could be regenerated by cycling to positive potentials.

Depending on the nature of the catalyst and reduction conditions, it is clear that a range of CO_2 electroreduction products are possible. Therefore, it is desirable to have a rapid means of identifying the product species and studying the electroreduction process. Techniques commonly used include mass spectrometry, gas chromatography, nuclear magnetic resonance (NMR) spectroscopy and combinations thereof [17]. However, most of these techniques involve analysis of the electrolyte solution off-line, with product generated at a given potential being determined by analysing the batch produced over a given integration time. This means that the dynamics of product formation is much harder to access and the calculated Faradaic efficiency is an average over the batch period. Therefore, there is a need to determine product formation as it occurs in real time and be able to perform experiments in which the reduction potential is dynamically varied.

The rotating ring-disc electrode (RRDE) has been extensively used to study the kinetics of a range of electrochemical systems and has the potential to provide an immediate indication of the amount and type of product from CO_2 electroreduction. Using a rotating assembly composed of a central disc electrode surrounded by a ring electrode, the product from the disc can be detected as it is swept outward by convection to the ring electrode [18]. In the case of CO_2 reduction at the disc, products can be detected if a sufficiently oxidising potential is applied at the ring electrode (Fig. 1).

There are two main ways of conducting an RRDE experiment: (i) scan the potential of the disc and hold the ring at a potential to detect product; (ii) hold the disc potential to sustain reaction and scan the ring potential. The former is useful for identifying the potential at which a certain product is generated at the disc and the latter provides a degree of characterisation of product/s formed at the disc by scanning the ring and using the potential as an indicator. The RRDE technique was used by Lates et al. to study the electrochemical reduction of CO_2 on polycrystalline gold, gold nanoparticles and gold@silver core-shell nanoparticles, with the product identified as being carbon monoxide [19]; but the technique is surprisingly underused in this area. In addition to providing a useful diagnostic function, the controlled hydrodynamics, which a rotating electrode imparts, also makes for a more controlled reaction environment where the supply of CO_2 (or its solution form) can be controlled/reproduced with more accuracy than a stationary electrode.

This study describes the use of copper(I) oxide nanoparticles (prepared using CHFS) as the active phase for the electroreduction of CO_2 using a RRDE in an appropriate solution. The RRDE is used to control the mass transfer of reactant to the electrode surface and, alongside NMR, as a means of studying the product species generated over a range of reduction potentials.

2. Experimental

2.1. Reagents

The following reagents were used: potassium hydroxide (anhydrous, 99.97% trace metals basis), copper sulphate pentahydrate (99.999% trace metals basis) and fructose powder (99%), potassium bicarbonate (ACS reagent, 99.7%, powder), 2-propanol (IPA, ACS reagent, 99.5%) and Nafion solution (9.81 wt% in water), potassium formate (ReagentPlus, 99%) and methanol (anhydrous, 99.8%) all from Sigma-Aldrich, Dorset, UK. Carbon monoxide was from CK Gas Limited.

2.2. Continuous hydrothermal flow synthesis (CHFS) of Copper(I) oxide and characterisation

Copper(I) oxide nanoparticles were synthesized using a lab-scale CHFS system, details of which are described in prior publications [14]. A schematic of the process can be found in Supplementary Fig. 1 (Fig. S1). Briefly, at room temperature solution of 0.1 M copper sulfate pentahydrate mixed with 1 wt% fructose was pumped (via pump 2 at 40 mL min^{-1}) to meet a room temperature solution of 0.2 M KOH (via pump 3 at 40 mL min^{-1}) under pressure in a T-piece mixer. The combined mixture was then rapidly mixed with a feed of supercritical water at 450 °C (via pump 1 at 80 mL min^{-1}) inside a confined jet mixer (CJM 1) as denoted in the diagram. The calculated mixing temperature at this point was ~335 °C. The CJM was designed to facilitate rapid turbulent mixing (calculated Reynolds number ~6900) of the feeds and prevent blockages. At the initial mixing point, nanoparticles were rapidly formed and following a residence of ~0.76 s, they were quenched in a second CJM using a feed of deionized water (delivered via pump 4 at 160 mL min^{-1}), with a Reynolds number of ~3300 in the second CJM (in between turbulent and laminar). The nanoparticles were then cooled further in flow via a pipe-in-pipe heat exchanger and subsequently continuously collected at the exit of the back-pressure regulator. The collected slurry was left to settle and the supernatant was decanted off. A nanoparticle paste was obtained that was then cleaned via three centrifugation and DI water

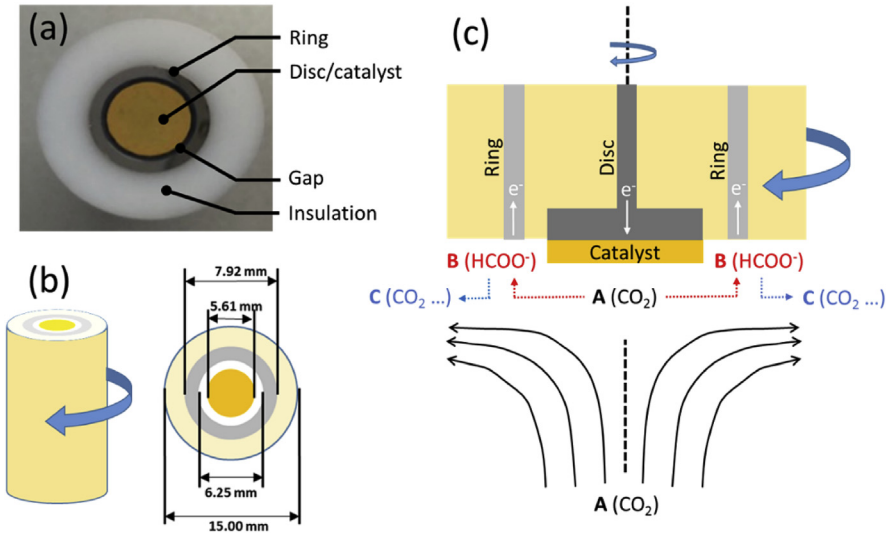

Fig. 1. (a) Labelled photo of RRDE with Cu_2O catalyst on the glassy carbon disc electrode and Pt ring; (b) key dimensions of the RRDE; and (c) scheme of RRDE operation showing reduction of CO_2 at the disc to formate, with subsequent oxidation at the ring, as an example.

washing cycles in 50 mL Falcon tubes (3700 rpm) until the conductivity of the solution was below 50 μS (measured using conductivity meter (Hanna instruments model H198311, Bedfordshire, UK). The concentrated slurry was then freeze-dried with slow heating of the frozen sample from − 40 °C to 25 °C (VirTis Genesis 35 XL Lyophilizer at $\times 10^{-7}$ MPa for 24 h).

2.3. Characterisation of Copper(I) oxide

The copper(I) oxide nanoparticles were examined by powder X-ray diffraction (PXRD) (STOE STADI P with Mo X-ray source). Surface analysis was conducted using Thermo Scientific K-Alpha X-ray photoelectron spectrometer. Survey scans were conducted at a pass energy of 150 eV and high-resolution region scans were conducted at 50 eV. The XPS spectra were processed using CASA™ software. The binding energy scale was calibrated by the C 1s peak at 285.0 eV. The morphology and size analysis was carried out using high-resolution transmission electron microscopy (HRTEM). Images were obtained on a JEOL JEM 2100 TEM with 200 keV accelerating voltage and a $LaBF_6$ filament. HRTEM samples were prepared by dispersing the particles in methanol followed by ultrasonication before dropping the resulting dispersion onto 300 mesh holey copper film grids (Agar Scientific, Stansted UK). Particle size distribution was determined by measuring the diameter of 150 particles from TEM images.

2.4. Ink preparation

The copper(I) oxide catalyst of 8.7 mg was mixed with 32.4 μL Nafion solution (9.61 wt% in water), 3.0 mL DI H_2O, and 7.0 mL IPA, to form the catalytic ink which was sonicated in a sonic bath for one hour. The catalyst particles were well-dispersed after sonicating, forming a pale yellow ink.

2.5. Electrode preparation

Catalyst ink was drop-coated on the surface of the glassy carbon disc electrode. A total ink volume of 30 μL was coated on the glassy carbon disc electrode, to achieve a final loading of 26 μg cm^{-2} (0.026 mg cm^{-2}). The counter electrode was a platinum mesh of 1 × 1 cm attached with platinum wire (diameter = 0.2 mm) (Sigma-Aldrich, UK), and the reference electrode was a reversible hydrogen electrode, RHE (Hydroflex, Gaskatel, Germany).

2.6. Electrochemical testing

A jacketed three-electrode electrochemical cell (Adams & Chittenden, USA) was used for all experiments at room temperature. Potassium bicarbonate solution (0.5 M) was prepared as the electrolyte. The original pH of 0.5 M $KHCO_3$ electrolyte was 8.1 and it was reduced to 7.1 after CO_2 saturation for 40 min. A rotator (Pine Research Instrumentation, USA) was used to control the rotation and a bi-potentiostat (Iviumstat, Ivium Technology, The Netherlands) was used to perform and monitor the electrochemical testing. Rotating ring-disc electrode (Pine Research Instrumentation, USA) was used as working electrode. It contained a glassy carbon disc electrode and a platinum ring electrode with a PTFE gap in between (Fig. 1). Electrochemical reduction of CO_2 took place on the disc electrode where the ring electrode could then directly oxidise any possible product generated from the disc electrode. The disc electrode had an area of 0.2475 cm^2 and the ring electrode was 0.1866 cm^2. The RRDE electrode was calculated to have a 38.5% collection efficiency.

As different products from the electroreduction of CO_2 are possible, the Pt ring electrode's electrochemistry was characterised in 80 ml 0.5 M $KHCO_3$ electrolyte containing: methanol (10.0 mL), potassium formate (5.0 g) and saturated with carbon monoxide.

Prior to the electrochemical reduction of CO_2, the system was initially degassed with N_2 for 40 min at a flow rate of 100 mL min^{-1}. The electrolyte was then saturated with CO_2 after bubbling it for 40 min with a flow rate of 100 mL min^{-1}. In each case, cyclic voltammetry scans were performed while the disc electrode was scanned from 0 to −1.2 V vs RHE, and ring electrode was held at different potentials in the range +0.7 V and +1.1 V vs RHE with 0.1 V intervals. During this set of experiments, CO_2 could be reduced to the product and the ring electrode could detect the product at the same time by oxidising it at a certain potential on the ring electrode. For all experiments, the RRDE rotation speed was set to 1500 rpm in order to have controlled hydrodynamics with reproducible flow of reactant to the disc surface and subsequent product to the ring electrode.

In the second set of experiments, the ring electrode was scanned

in the range 0.0–1.3 V vs RHE, while the disc electrode was held at various reduction potentials in the range −0.4 to −0.9 V vs RHE (with 0.1 V intervals). In this set of experiments, the product was generated consistently at the disc electrode, while the ring electrode could detect the product from its oxidation current/potential.

Chronoamperometry tests were performed on the disc electrode in the range −0.4 to −0.9 V vs RHE with 0.1 V potential intervals to determine the Faradaic efficiency at each point. Each potential was held for one hour to accrue product in the cell and the ring was not activated during this period (to avoid product oxidation). Samples of the electrolyte (2.0 mL) were collected after chronoamperometry tests and NMR analysis was performed. According to the chronoamperometry tests, charge passed through the disc at each potential hold can be calculated by taking the integral of current over time.

For the NMR analysis, samples were added to the NMR tube with D_2O as the base solution and analyses performed using a 600-MHz NMR spectrometer (Bruker Avance III 600 Cryo). The NMR spectrometer has a detection limit of 1.49 mg l^{-1} for formate and 3.3 mg l^{-1} for methanol. Detection limit for gaseous products depend on the saturation level. The NMR analysis could provide qualitative identification based on ^1H analysis as well as quantitative analysis based on controlled calibration. Therefore, Faradaic efficiency could be calculated for a given product based on the amount generated and the charged passed according to Faraday's law.

3. Results and discussion

3.1. Characterisation of the catalyst

Copper(I) oxide nanoparticles were synthesized using a lab-scale CHFS reactor. A 0.1 M copper sulfate pentahydrate with 1 wt % fructose and 0.2 M KOH were used to produce the nanoparticles. The resulting yellow coloured slurry was cleaned and the solids were freeze-dried. The powder XRD pattern confirmed the presence of pure phase Cu_2O with a cubic structure, similar to the standard reference pattern for Cu_2O (JCPDS 01-071-3645) (Fig. 2 a)). The pattern showed the existence of only the Cu_2O phase with no secondary phases from CuO or Cu metal, confirming that the short residence time within the first CJM was sufficient to form pure-phase Cu_2O. The sharp peaks indicated the particles were crystalline in nature and the application of the Scherrer equation resulted in a crystallite size of 35 nm. Surface analysis of the Cu_2O sample showed the existence of Cu_2O (peak $2p_{3/2}$ at 932.3 eV) but also the presence of CuO phase, as confirmed from the satellite peaks and the presence of the $2p_{3/2}$ peak at 934.8 eV corresponding to CuO (Fig. 2 b)). The existence of CuO in the surface analysis suggests the presence of an amorphous CuO layer on the surface of the Cu_2O nanoparticles, which was likely not seen in the XRD due to its amorphous nature. This is expected as the surface undergoes oxidation from Cu_2O to form amorphous CuO due to the unstable Cu^+ oxidation state. As-synthesized nano-powders were also characterised by transmission electron microscopy (TEM) (Fig. 2 c)) where round crystalline nanoparticles were observed. Bersani et al. synthesized CuO nanoparticles using CHFS where the nanoparticles were crystalline with diameter of 11 ± 4 nm from TEM [14]. The electrochemical behaviour of the as-prepared Cu_2O nanoparticles was subsequently examined to evaluate the performance of Cu_2O nanoparticles for CO_2 conversion.

3.2. Electrochemical calibration of the ring electrode for possible products

The RRDE offered the possibility of identifying disc reduction products at the ring. To do this, an element of ring 'calibration' was required by determining the electrochemistry of possible product species at the Pt ring. Cyclic voltammetry scans of the ring electrode were performed on the range 0.0–1.4 V vs RHE in CO_2-saturated 0.5 M $KHCO_3$ 'blank' electrolyte and that containing saturated carbon monoxide, potassium formate (0.59 M) and methanol (0.1 M) (Fig. 3).

A characteristic Pt-type CV was obtained when there was no additional substance in the electrolyte. Daubinger et al. reported the electrochemistry of polycrystalline platinum in different electrolytes [20]. In phosphate buffered saline electrolyte with a neutral pH, the PtO reduction peak took place at 0.75 V vs RHE, which matched the Pt 'calibration' in 0.5 M $KHCO_3$ electrolyte. Formate oxidation took place with a peak at 0.93 V vs RHE, and is thought to be oxidised to CO_2 via a dehydrogenation route. CO can also be generated during the indirect dehydration process of formate oxidation [21]. On the reverse scan, the peak at 0.82 V vs RHE was attributed to formate oxidation taking place on the re-activated ring electrode. Zhang et al. outlines the possibility of another smaller feature at a slightly lower potential on the reverse scan due to decreased rate of formate oxidation into CO_2, and increased rate of CO produced from formate [22].

Methanol oxidation was detected with a peak at 1.03 V vs RHE. During the reverse scan, a peak at 0.9 V vs RHE indicated the re-activation of the Pt ring associated with reduction of PtO, leading

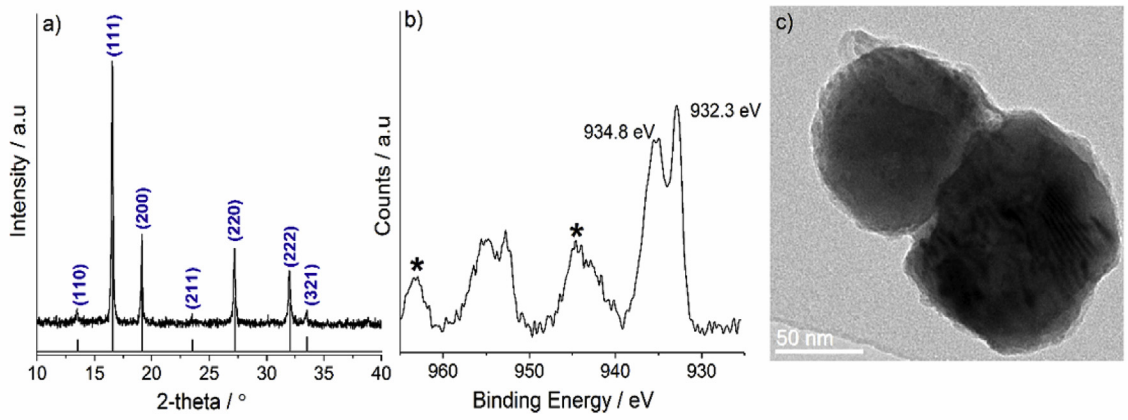

Fig. 2. Structural characterisation of Cu_2O nanoparticles as synthesized by CHFS a) PXRD of Cu_2O nanoparticles in agreement with JCPDS 01-071-3645, b) high-resolution Cu 2p XPS scan of Cu_2O sample and c) TEM image of Cu_2O nanoparticles.

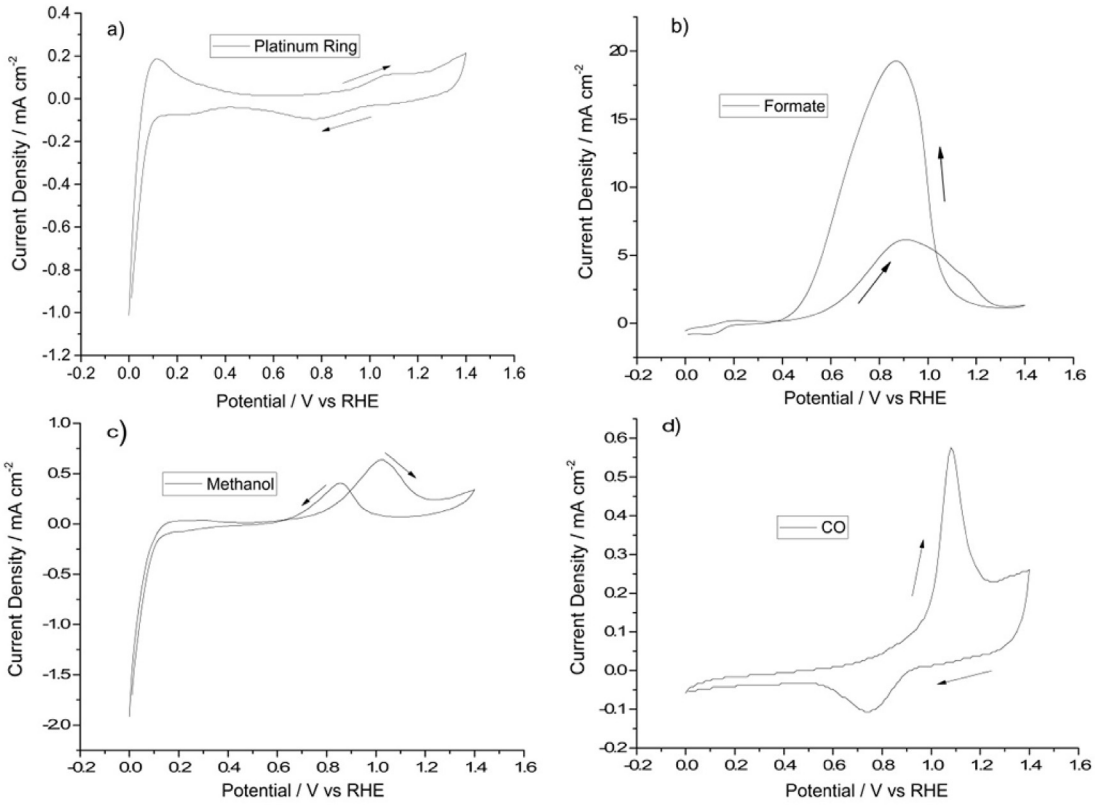

Fig. 3. Cyclic voltammetry scans for calibration of possible products from CO_2 reduction in CO_2-saturated 0.5 M $KHCO_3$ electrolyte. a) Ring Pt electrode cyclic voltammetry (no species added) and that containing: b) formate; c) methanol and d) CO. The ring was scanned in the range 0.0–1.4 V vs RHE. Disc electrode was off. Rotation speed of 1500 rpm was used. Scan rate: 100 mV s^{-1}.

to further oxidation of methanol, as described by Hofstead-Duffy et al. [23].

A carbon monoxide electrochemical oxidation (stripping) peak was observed at 1.1 V vs RHE for this CO-saturated electrolyte. Garcia et al. found CO oxidation at 0.8 V vs RHE in 0.1 M NaOH solution [24]. Considering the difference in pH between the NaOH alkaline electrolyte (pH ≈ 12) and that of this CO_2-saturated $KHCO_3$ electrolyte matrix, the CO oxidation would be expected to be ~1.09 V vs RHE, in accordance with that observed here.

3.3. Electrochemical reduction of CO_2

In order to use the RRDE to help identify oxidation product types, quantity and efficiency, three approaches were taken. The first approach scans the disc potential through the CO_2 reduction window and collects the ring current at a number of fixed

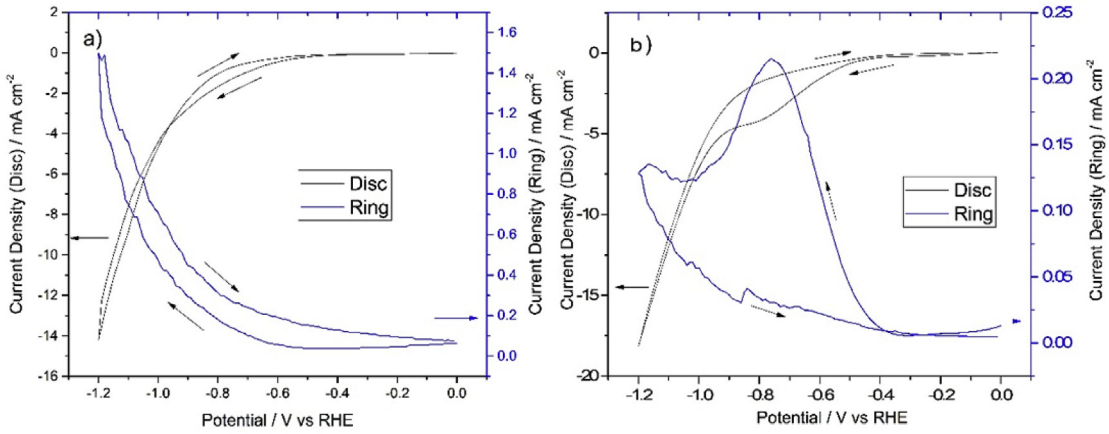

Fig. 4. Cyclic voltammetry scans of the RRDE. Disc electrode was scanned between 0 and −1.2 V vs RHE, the ring electrode was held at +0.9 V vs RHE. a) Initial CV scan for N_2 purged electrolyte. Ring electrode was held at +0.9 V vs RHE. B) CV scan for the system after CO_2 saturation with the ring held at +0.9 V vs RHE. The experiments were all performed at room temperature. Scan rate: 100 mV s^{-1}. Constant rotation (1500 rpm) was used.

potentials. This allowed the potential (range) of CO_2 reduction to be determined with some information inferred about the nature of the product formed. The second approach held the disc at a potential where substantial CO_2 reduction was likely to occur (determined using the first approach) and scanning the ring potential was conducted to characterise the product species, with comparison to the calibration tests in Section 3.2. Finally, batch reduction was performed with product species quantification using NMR compared with the total charge passed to determine the Faradaic efficiency.

3.3.1. Scan disc electrode, hold ring electrode (disc-scan)

Cyclic voltammetry was performed on N_2-purged electrolyte, with the disc electrode scanned from 0 to −1.2 V vs RHE and ring electrode held at +0.9 V vs RHE. The same process was repeated in CO_2-saturated electrolyte, with the ring held at various oxidation potentials.

Fig. 4(a) shows the N_2-purged reduction profile; the disc/ring show characteristic hydrogen evolution/reduction profiles which contrast with the CO_2-containing voltammetry, where CO_2 reduction (in the range −0.5 V to −0.9 V vs RHE) and subsequent product oxidation is clearly seen, with a peak ring current of 0.23 mA cm^{-2} at a disc potential of −0.75 V vs RHE (Fig. 4(b)).

A ring hold potential of 0.9 V vs RHE corresponded to the peak formate oxidation potential (Fig. 3(b)). When the ring hold potential was increased to 1.0 V vs RHE (close to the maximum methanol peak potential – Fig. S2(c)), the peak ring current *decreased* to 0.07 mA cm^{-2}. Also, as the ring potential was below that for CO stripping, if CO were a disc product, the Pt ring would have been expected to be poisoned (blocked). However, the ring current was stable with time (over the course of 1 h) and increasing the ring current to 1.1 V vs RHE (close to the CO stripping potential) resulted in further decrease in the ring current to 0.04 mA cm^{-2}. These electrochemical results suggested that formate was the major CO_2 reduction product for this catalyst/electrolyte system.

3.3.2. Hold disc electrode, scan ring electrode (ring-scan)

The ring electrode was scanned in the range 0.0–1.3 V vs RHE

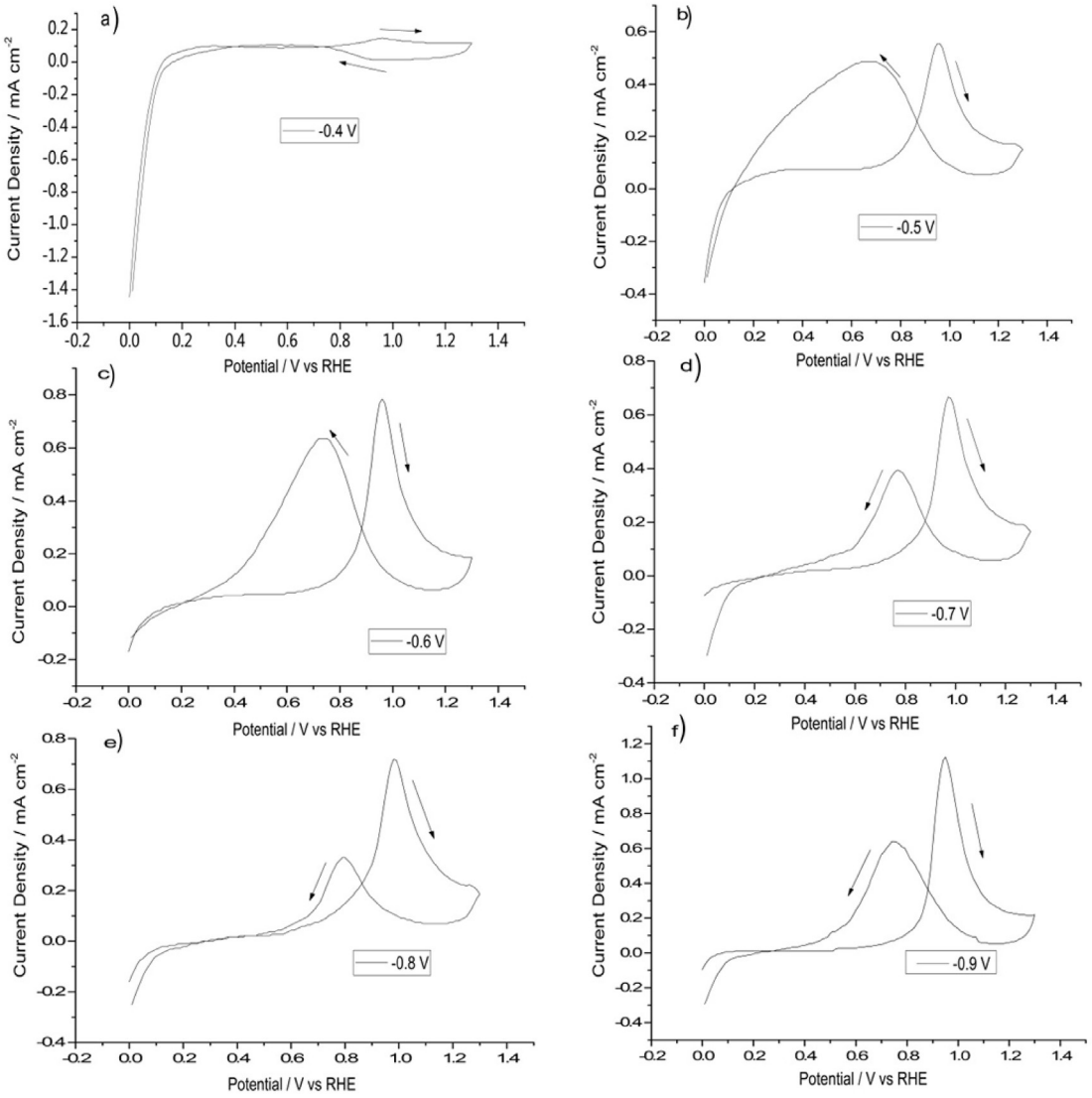

Fig. 5. Cyclic voltammetry scan of the ring electrode when the disc electrode was held from −0.4 V to −0.9 V vs RHE. Ring electrode was scanned between 0 and 1.3 V vs RHE. A constant rotation of 1500 rpm was applied in each case. Scan rate: 100 mV s^{-1}.

with scan rate of 100 mV s^{-1}, and the disc electrode was held at certain potentials where it could generate products continuously (identified from Fig. 4(b) to be over the range −0.4 to −0.9 V vs RHE (0.1 V intervals). The oxidation peaks of the product on the ring electrode at different potentials could also be related to the efficiencies of products being produced. Fig. 5 shows the change of the ring scans while the disc was held at different potentials.

As shown in Fig. 5(a), the ring electrode did not show an obvious oxidation peak when the disc electrode was held at −0.4 V vs RHE, indicating that product is not generated at this potential. As the holding potential of the disc electrode became more negative, the oxidation peak of the product became apparent. When the disc electrode was held at −0.5 V vs RHE, the electro-oxidation peak was observed at +0.94 V vs RHE with a current density of 0.58 mA cm^{-2}. With increasingly negative disc potential, a single well-defined ring peak was observed at +0.94 V vs RHE, indicating that a consistent product type was being generated across the range of disc reduction potentials. This was consistent with the production of formate, as implied in Section 3.3.1 and calibrated for at +0.93 V vs RHE in Fig. 3(b).

From Fig. 5(b)–(f), the reverse scan showed an oxidation peak on the re-activated ring electrode. In Fig. 5(b), the re-activated ring oxidation peak at −0.73 V vs RHE was large and broad; however, the peak reduces from Fig. 5(c)–(e). The size of the peak then increased in Fig. 5(f) when the disc electrode was held at −0.9 V vs RHE.

Okamoto et al. have shown that for formic acid, the current in the negative-going potential sweep is strongly influenced by the accessibility of water to support the oxidation process, the current increasing with water concentration. The increase in current is associated with increasing number of vacant sites produced by the oxidation of adsorbed CO with water, hydroxide or oxide on platinum [25]. Increasing formate generation with more negative potential reduces the relative availability of water at the ring; this is taken to account for the decrease in negative-going current observed in Fig. 5.

3.3.3. *Batch reduction and determination of Faradaic efficiency*

For comparison with electrochemical results and to determine the Faradaic efficiency, chemical characterisation and quantification of the product species was performed using NMR of the electrolyte after batch electrolysis. Chronoamperometry was performed while the disc was held at specific potentials in the range −0.4 to −0.9 V vs RHE (0.1 V intervals and holding for one hour at each potential). The ring electrode was switched off during chronoamperometry tests to avoid conversion of any product species. An example of the NMR spectra obtained (Fig. (S3)) and its interpretation is provided in the Supplementary Information. Of the possible expected products, only formate was detected, regardless of the disc hold potential. As noted by Le et al. [8], the formation of formic acid in a two-electrons and two-protons reaction, is more facile compared to the formation of methanol from CO_2 in a six-electrons and six-protons reaction. The Faradaic efficiency of formate production over the range −0.4 to −0.9 V vs RHE, was calculated as described in Section 2.6 and shown in Fig. 6.

In agreement with the electrochemical characterisation, at −0.4 V vs RHE, there was almost no formate generated and the Faradaic efficiency at this point was negligible, the current was dominated by the onset of H_2 evolution. The Faradaic efficiency increased to 44% at −0.6 V vs RHE after which it decreased slightly (or plateaus) at −0.7 V (36%) before reaching a maximum of 66% at −0.8 V vs RHE.

As already mentioned, Gupta et al. reported production of formic acid from the electrochemical reduction of CO_2 in 0.5 M $KHCO_3$ electrolyte using a CuO catalyst [15]. They found the highest

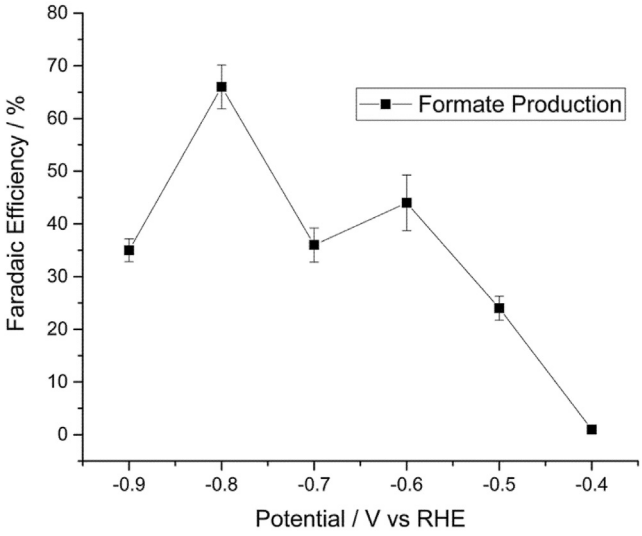

Fig. 6. Faradaic efficiency of formate produced from CO_2 reduction at the disc of a RRDE. Potassium bicarbonate of 0.5 M was the electrolyte, Cu_2O was the catalyst. The disc electrode was held between −0.4 V and −0.9 V vs RHE for one hour for each holding potential.

Faradaic efficiency to be 61% at −1.4 V vs Ag/AgCl for an electrode catalyst loading of 0.3 mg cm^{-2}, which is an order of magnitude larger than the catalyst loading on the disc electrode (0.026 mg cm^{-2}) in this study. An increase in Faradaic efficiency to 66% for a catalyst with an order of magnitude lower loading indicates that this is a promising CO_2 conversion catalyst. In addition, the rotating ring-disc electrode approach is an efficient technique in terms of electrochemical reduction of CO_2 with fast reactant transport and accurate detection of the product while the experiments were running.

4. Conclusion

Nanoparticles of copper(I) oxide produced using a continuous hydrothermal flow synthesis method proved to be an effective electrocatalyst for the reduction of CO_2 exclusively to formate with a maximum Faradaic efficiency of 66% at −0.8 V vs RHE.

In this work, the ring electrode has been used to identifying the products from CO_2 reduction. Formate was consistently detected and identified as the product from electrochemical reduction of CO_2 using Cu_2O catalyst in 0.5 M $KHCO_3$ solution under room temperature. When the disc electrode was scanned, the ring electrode detected the oxidation peak when it was held at +0.9 V vs RHE which indicated that the product from CO_2 reduction was oxidised at around this potential on the ring electrode. This was then confirmed by scanning the ring electrode with disc electrode held at different potentials where consistent oxidation peak at +0.94 V vs RHE on the ring electrode was observed. This indicated that formate was the product from CO_2 reduction. The results could also be compared to the calibration result of formate oxidation in CO_2-saturated 0.5 M $KHCO_3$ where formate oxidation took place at +0.93 V vs RHE which could also confirm the formation of formate from electrochemical reduction of CO_2. From between −0.5 V vs RHE to −0.9 V vs RHE, formate was detected as the exclusive product from reduction of CO_2. This was then confirmed by the results from NMR spectroscopy. Therefore, the RRDE technique has been shown to be a useful tool in characterising the electroreduction process and can provide both qualitative and quantitative information about the CO_2 reduction products.

Acknowledgements

The authors would like to acknowledge the EPSRC for supporting this research through (EP/K035355/2, EP/R023581/1, EP/P009050/1, EP/K014706/2, EP/K038656/1, EP/M014371/1) and the EPSRC Centre for Doctoral Training in Molecular Modelling and Materials Science (EP/L015862/1) for supporting the Ph.D. studentship of Zhu. JAD and MB acknowledge funding from the ESPRC (EP/K035355/2). PRS acknowledges funding from the Royal Academy of Engineering.

Appendix A. Supplementary data

Supplementary data related to this article can be found at https://doi.org/10.1016/j.electacta.2018.07.025.

References

[1] R. Schmalensee, T.M. Stoker, R.A. Judson, World carbon dioxide emissions: 1950 – 2050, Rev. Econ. Stat. (1998) 15–27.
[2] J.H. Mercer, West antarctic ice sheet and CO_2 greenhouse effect: a threat of disaster, Nature (1978) 321–325.
[3] S.C. Roy, O.K. Varghese, M. Paulose, C.A. Grimes, Toward solar fuels: photo catalytic conversion of carbon dioxide to hydrocarbons, Am. Chem. Soc. ACS Nano 4 (3) (2010) 1259–1278.
[4] Q. Zhang, C.-F. Lin, Y.H. Jing, C.-T. Chang, Photocatalytic Reduction of carbon dioxide to methanol and formic acid by graphene-TiO2, J. Air Waste Manag. Assoc. 64 (2014) 578–585.
[5] K. Hara, A. Kudo, T. Sakata, Electrochemical reduction of carbon dioxide under high-pressure on various electrodes in an aqueous electrolyte, J. Electroanal. Chem. 391 (1995) 141–147.
[6] C. Delacourt, P.L. Ridgway, J.B. Kerr, J. Newman, Design of an electrochemical cell making syngas ($CO + H_2$) from CO_2 and H_2O reduction at toom temperature, J. Electrochem. Soc. 155 (2008) B42–B49.
[7] H. Noda, S. Ikeda, Y. Oda, K. Imai, M. Maeda, K. Ito, Electrochemical Reduction of Carbon Dioxide at Various Metal Electrodes in Aqueous Potassium Hydrogen Carbonate Solution, The Chemical Society of Japan, 1990, pp. 2459–2462.
[8] M. Le, M. Ren, Z. Zhang, P.T. Sprunger, R.L. Kurtz, J.C. Flake, Electrochemical reduction of CO_2 to CH_3OH at copper oxide surfaces, J. Electrochem. Soc. 158 (5) (2011) E45–E49.
[9] S. Ohya, S. Kaneco, H. Katsumata, T. Suzuki, K. Ohta, Electrochemical reduction of CO_2 in methanol with aid of CuO and Cu_2O, Catal. Today (2009) 329–334.
[10] D. Ren, Y. Deng, A.D. Handoko, C.S. Chen, S. Malkhandi, B.S. Yeo, Selective electrochemical reduction of carbon dioxide to ethylene and ethanol on Copper(I) oxide catalysts, Am. Chem. Soc. ACS Catal. 5 (2015) 2814–2821.
[11] J.A. Darr, J. Zhang, N.M. Makwana, X. Weng, Continuous hydrothermal synthesis of inorganic nanoparticles: applications and future directions, Chem. Rev. 117 (17) (2017) 11125–11238.
[12] M. Chen, C.Y. Ma, T. Mahmud, J.A. Darr, W.Z. Wang, Modelling and simulation of continuous hydrothermal flow synthesis process for nano-materials manufacture, J. Supercrit. Fluids 59 (2011) 131–139.
[13] V. Middelkoop, C.J. Tighe, S. Kellici, R.I. Gruar, J.M. Perkins, S.D.M. Jacques, P. Barnes, J.A. Darr, Imaging the continuous hydrothermal flow synthesis of nanoparticulate CeO_2 at different supercritical water temperatures using in-situ angle-dispersive diffraction, J. Supercrit. Fluids 87 (2014) 118–128.
[14] M. Bersani, K. Guptai, A.K. Mishra, R. Lanza, R. Taylor, H. Islam, Nathan Hollingsworth, C. Hardacre, N.H. de Leeuw, J.A. Darr, Combined EXAFS, XRD, DRIFTS, and DFT study of nano copper-based catalysts for CO_2 hydrogenation, ACS Catal. (2016) 5823–5833.
[15] K. Gupta, M. Bersani, J.A. Darr, Highly efficient electro-reduction of CO_2 to formic acid by nano-copper, J. Mater. Chem. A 4 (2016) 13786.
[16] L. Wang, K. Gupta, J.B.M. Goodall, J.A. Darr, K.B. Holt, In situ spectroscopic monitoring of CO2 reduction at copper oxide electrode, Faraday Discuss 197 (2017).
[17] C.W. Li, M.W. Kanan, CO_2 reduction at low overpotential on Cu electrodes resulting from the reduction of thick Cu_2O films, J. Am. Chem. Soc. 134 (2012) 7231–7234.
[18] H.K. Kuiken, E.P.A.M. Bakkers, H. Lighthart, J.J. Kelly, The rotating ring-ring electrode, theory and experiment, J. Electrochem. Soc. 147 (2000) 1110–1116.
[19] V. Lates, A. Falch, A. Jordaan, R. Peach, R.J. Kriek, An electrochemical study of carbon dioxide electroreduction on gold-based nanoparticles catalysts, Electrochim. Acta 128 (2014) 75–84.
[20] P. Daubinger, J. Kieninger, T. Unmussig, G.A. Urban, Electrochemical characteristics of nanostructured platinum electrodes – a cyclic voltammetry study, Phys. Chem. Chem. Phys. 16 (2014) 8392–8399.
[21] Y. She, Z. Lu, W. Fan, S. Jewell, M.K.H. Leung, Facile preparation of PdNi/rGO and its electrocatalytic performance towards formic acid oxidation, J. Mater. Chem. A 2 (2014) 3894–3898.
[22] J. Zhang, PEM Fuel Cell Electrocatalysts and Catalyst Layers: Fundamentals and Applications, Springer-Verlag London Limited, 2008. Chapter 4.2.2 – Formic Acid Electrooxidation.
[23] A.M. Hofstead-Duffy, D.J. Chen, S.G. Sun, Y.J. Tong, Origin of the current peak of negative scan in the cyclic voltammetry of methanol electro-oxidation on Pt-Based electrocatalysts: a revisit to the current ratio criterion, J. Mater. Chem. 22 (2012) 5205.
[24] G. Garcia, M.T.M. Koper, Stripping voltammetry of carbon monoxide oxidation on stepped platinum single-crystal electrodes in alkaline solution, Phys. Chem. Chem. Phys. 10 (2008) 3802–3811.
[25] H. Okamoto, T. Gojuki, N. Okana, T. Kuge, M. Morita, A. Maruyama, Y. Mukouyama, Oxidation of formic acid and methanol and their potential oscillations under No or little water conditions, Electrochim. Acta (2014) 385–395.